*Int. J. Electrochem. Sci.*, 14 **(2019)** 9695 – 9703, doi: 10.20964/2019.10.22

International Journal of
ELECTROCHEMICAL
SCIENCE
www.electrochemsci.org

# Investigation of $Al_2O_3$ Crucible Contamination induced by extra $Li_2CO_3$ during $Li_7La_3Zr_2O_{12}$ Solid Electrolyte Sintering process

*Weijie Lan*[1], *Dongliang Lu*[2], *Ruirui Zhao*[1,*], *Hongyu Chen*[1,*]

[1] School of Chemistry and Environment, South China Normal University, Guangdong Guangzhou, 510006, China
[2] Guangdong Polytechnic of Environmental Protection Engineering, Foshan, 528216, China
[*]E-mail: zhaoruirui@m.scnu.edu.cn, hychen@scnu.edu.cn

*Received:* 23 May 2019 / *Accepted:* 29 July 2019 / *Published:* 30 August 2019

$Al_2O_3$ crucible is commonly used during the sintering process of $Li_7La_3Zr_2O_{12}$ pellets, which always introduces unintentional Al-containing impurities to the final product. Rare investigations are focused on the mechanism of this crucible contamination up to now. Based on the study in this work, it is found that the extra $Li_2CO_3$ in the $Li_7La_3Zr_2O_{12}$ powder is a crucial factor in forming this kind of Al-containing impurities in the obtained pellets. The pyrolytic $Li_2O$ from $Li_2CO_3$ will react with $Al_2O_3$ at high temperature, forming liquid Li-Al-O eutectic and further promoting the dissolution of aluminum oxide crucible. Besides, the extra $Li_2CO_3$ can also affect the compactness and the distribution of Al element in the pellets, resulting in crystal structure transformation.

**Keywords:** $Li_2CO_3$; $Li_7La_3Zr_2O_{12}$ garnet; gain conductivity; solid-state electrolyte

## 1. INTRODUCTION

Nowadays, replacing the flammable organic liquid electrolyte with much safer inorganic solid-state electrolyte is considered as an effective way to solve the safety issues encountered by lithium ion batteries [1-3]. Among all solid electrolytes, Li-containing garnet $Li_7La_3Zr_2O_{12}$ (LLZO) has attracted widest attention due to its relatively high conductivity, chemical stability to metallic lithium and wide electrochemical stability voltage window [4-5]. LLZO is usually synthesized by traditional solid-state reaction method due to the scalable synthesis process and low cost. However, the products from solid-state method exhibit low reproducibility and controllability, arise from the volatilization of Li sources at higher temperatures [6] or uncontrollable Al contamination from crucible [7-8]. Usually, adding over-stoichiometric Li sources in the sintering process is considered as an effective strategy to offset the Li loss [6], however, when it comes to $Al_2O_3$ crucible contamination, no helpful methods have been reported due to the unclear reaction mechanism between the sample and crucible. It is commonly agreed

in previous works that amorphous Li-Al-O phase will generate during high-temperature sintering process [9-14] along with the formation of $LiAlO_2$ and $LiAl_5O_8$ impurities. Understanding the generation process and effecting factors of the formed Li-Al-O eutectic is vital in figuring out the crucible contamination mechanism, which is also helpful in realizing the performance repeatability of LLZO by solid-state method.

In this work, we tried to investigate the role of $Li_2CO_3$ in this kind of crucible contamination. It is reported before [15-16] that $Li_2CO_3$ can be generated under humid air based on the following equations, so we put the LLZO powder under humid environment for 5 days and employ it as the raw material to prepare LLZO solid electrolyte. Extra $Li_2CO_3$ are also added into the inert gas-protected LLZO powder to obtain pellets.

$$Li_{56}La_{24}Zr_{16}O_{96}(s) + H_2O(g) = Li_{54}La_{24}Zr_{16}O_{95}(s) + 2LiOH \quad (1)$$

$$Li_{56}La_{24}Zr_{16}O_{96}(s) + CO_2(g) = Li_{54}La_{24}Zr_{16}O_{95}(s) + Li_2CO_3 \quad (2)$$

$$2LiOH + CO_2(g) = H_2O + Li_2CO_3 \quad (3)$$

Results from this research indicate that the contamination of crucible is very sensitive to extra lithium source, while minute dopant of Al in the garnet is beneficial for increasing the electron conductivity, and higher Al concentration will bring in deteriorated performance of the solid electrolytes.

## 2. EXPERIMENTAL SECTION

### *2.1 Synthesis of LLZO powders*

The LLZO powders were synthesized by a conventional solid-state reaction. $Li_2CO_3$ (Aladdin, AR), $ZrO_2$ (Aladdin, 99.99%), and $La_2O_3$ (Aladdin, 99.99%) were used as raw materials. Before the synthesis, the small amount of moisture and adsorbed $CO_2$ were removed from $La_2O_3$ by heat treatment at 900 °C for 6 h. The raw materials were mixed according to the stoichiometric ratio of $Li_7La_3Zr_2O_{12}$, and 10% excess of lithium source was added to compensate the lithium loss during high-temperature sintering. The powders were ball milled with isopropyl alcohol (IPA) at a speed of 500 rpm for 24 h, then dried at 100 °C by using a vacuum drying oven. Pressing the powders into 25mm diameter pellets and then put the pellets into alumina crucible, sintering the pellets at 900 °C for 12 h and then grinding the sintered pellets after their cooling down and the obtained powders were stored in argon-filled glove box.

### *2.2 Synthesis of LLZO pellet*

The as-prepared LLZO powders were divided into four parts, while three of them were added with 0 wt.% $Li_2CO_3$, 1 wt.% $Li_2CO_3$, and 5 wt.% $Li_2CO_3$ under the protection of inert atmosphere, respectively. The remaining part was exposed directly to moist air (relative humidity is about 70%) for 5 days. The powders were pressed into 15 mm diameter pellets and sintered for 6 h at 1175 °C in an alumina crucible. The obtained pellets were named as 0%LC-LLZO, 1%LC-LLZO, 5%LC-LLZO and 5D-LLZO, respectively, as shown in scheme 1.

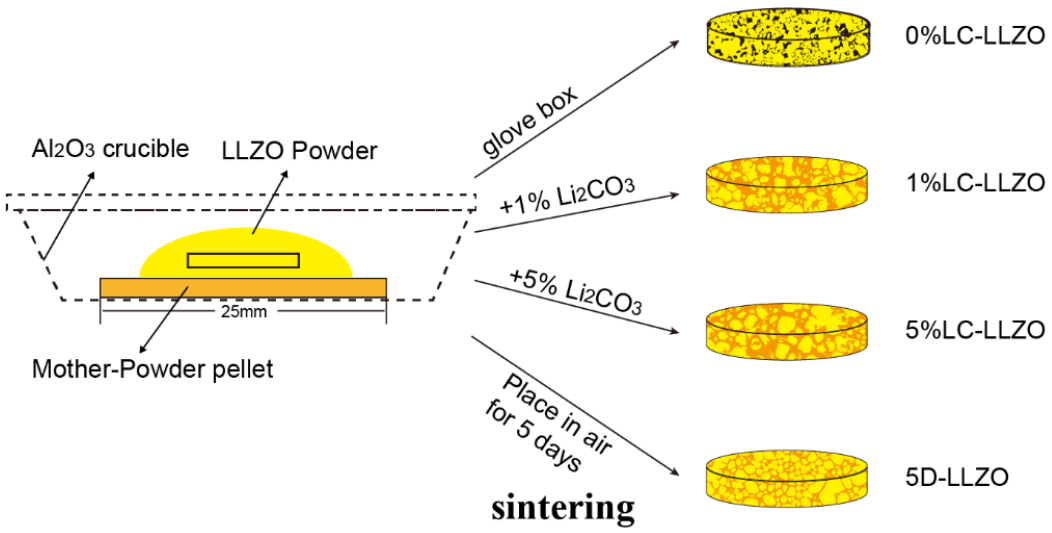


**Scheme 1**. The experimental design in this work

*2.3 SEM/EDX*

Scanning electron microscope (SEM) images were taken by using a Phenom Pro X device to study the grain size, morphology, and the chemical homogeneity (*i.e.*, the distribution of Al, La, Zr) was obtained by using an energy-dispersive X-ray spectroscopy (EDX) measurement. For SEM characterization, the pellets need to be polished with emery paper to clean up the surface of pellets in advance.

*2.4 XRD*

X-ray diffraction (XRD) patterns were recorded by an Ultima IV X- diffractometer using Cu $K_\alpha$ radiation. Data were collected in a 2θ range between 10° and 70°. Special regard was given to the transformation of crystal structure of LLZO and generation of heterogeneous phases after adding little $Li_2CO_3$ and exposing to moist air. Evaluation of XRD data was performed by Rietveld refinement using the program GSAS.

*2.5 EIS*

The ionic conductivity was measured by electrochemical impedance spectroscopy (EIS) using Autolab (Type: PGSTAT302N). To measure the ionic conductivity of LLZO, Au/LLZ/Au Li-ion blocking cell was fabricated, where Au was sputtered on both of the top and bottom sides of the sample and act as ionically blocking electrodes. EIS were recorded with an AC amplitude of 100 mV and a frequency range from 1 MHz to 1 Hz.

*2.6 ICP*

The $Al^{3+}$ concentration of the samples was measured by inductive coupled plasma (ICP) optical emission spectroscopy (OES) using German Spectro Arcos MV. 50 mg of the samples was dissolved in concentrated sulfuric acid and diluted to 500 mg $L^{-1}$ to measure the content of $Al^{3+}$. The solution is diluted 100 times to measure the content of $Zr^{4+}$.

## 3. RESULTS AND DISCUSSION

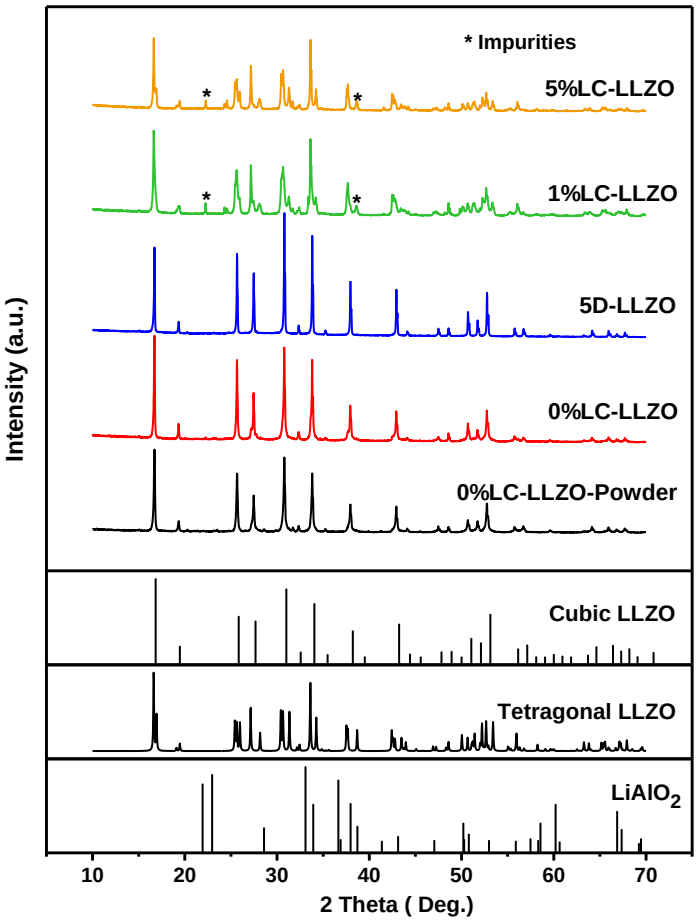


**Figure 2**. XRD patterns of the obtained powder and pellets

The XRD patterns of the LLZO powders are shown in *Figure 2*, which can be well indexed by a typical cubic phase structure with *Ia*-3*d* space group, and the lattice parameter was calculated to *a* = 12.9803 Å by using Rietveld refinement, corresponding well with previous report [17]. As can be seen, the obtained pellets exhibit different phase structures after second calcination, in detail, the 0%LC-LLZO and 5D-LLZO pellets can maintain the cubic phase, while the 1%LC-LLZO and 5%LC-LLZO ones exhibit tetragonal phase with obvious $LiAlO_2$ impurities. It seems that extra $Li_2CO_3$ in the mixture can affect the stability of the crystal phase of the obtained garnet, prompting the transformation of LLZO from cubic to tetragonal phase. However, no obvious difference observed for the 5D-LLZO specimen from the pristine pellet based on the XRD results, might due to the low content of $Li_2CO_3$.

*Figure 3* shows the morphologies of LLZO pellets with different compositions. Generally, compared with blank 0%LC-LLZO, all of the 5D-LLZO, 1%LC-LLZO and 5%LC-LLZO pellets exhibit more separated particles, resulting in much clear grain boundaries in these samples as seen from *Figure 2* panel *a* to *d* with dark and alloy-like impurities in-between. SEM-corresponding mapping was also employed to observe the composition of the impurities, while the distribution map of Al element is shown in Figure 3*e* to *h*. Apparently, the concentration of this kind of impurities increase with more $Li_2CO_3$ during the second sintering process. Based on XRD results and previous papers [19], this Al-containing impurity should be $LiAlO_2$, which arise from the reaction between $Li_2O$ vapor and $Al_2O_3$ crucible [16]. It can be seen that there is also $LiAlO_2$ impurity formed in 5D-LLZO sample, possibly due to the reaction between the $Li_2CO_3$ formed in moist air [20-23] and alumina crucible, as we discussed in the introduction. To summarize, $LiAlO_2$ impurity will form in the samples if there are extra $Li_2CO_3$ in the pellet sintering process, meaning that the extra $Li_2CO_3$ is the main reason for the impurity formation. Based on the $Li_2O$-$Al_2O_3$ phase diagram [24], the molten $Li_2O$ will generate from $Li_2CO_3$ at around 1109 ºC and then reacted with $Al_2O_3$ to form Li-Al-O eutectic liquid, which has a melting point of 1064 ºC. It can be also found that when no extra $Li_2CO_3$ added in the sintering process, as seen in Figure 3*a*, there are also little Al-containing products formed on the surface of the particles, which mainly resulted from the directly reaction between LLZO and trace $Li_2O$ vapor [16]. When there are extra $Li_2CO_3$ existed, either formed spontaneously or added artificially, the resultant Li-Al-O eutectic liquid as analyzed before will generate and tend to gather at the grain boundaries, forming uneven distribution of $LiAlO_2$ impurities after the pellets cooled to room temperature [25].

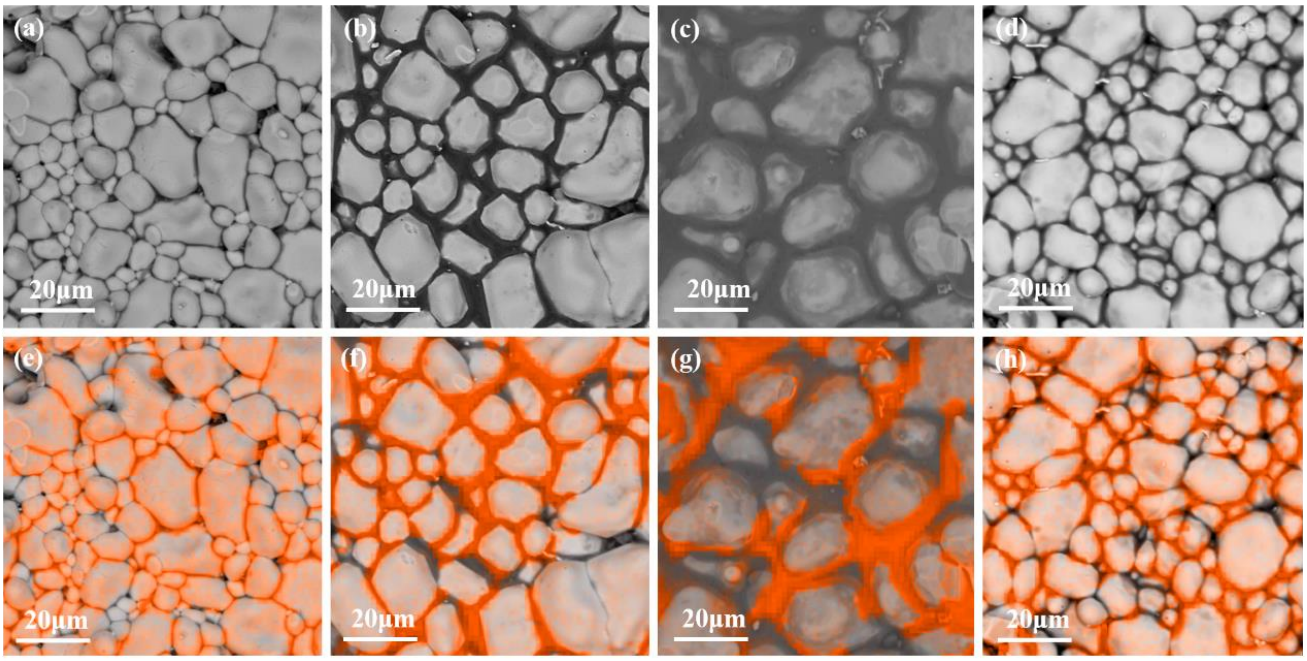


**Figure 3**. SEM images and the corresponding EDS-mapping of element Al for LLZO pellets obtained under different conditions: (a,e) 0%LC-LLZO; (b,f) 5D-LLZO; (c,g) 1%LC-LLZO; (d,h) 5%LC-LLZO;

**Table 1.** The elemental concentrations in the pellets determined by ICP and the calculated density data of the $Li_7La_3Zr_2O_{12}$ pellets.

| Sample ID | Al | Zr* | Diameter (cm) | Mass (g) | Thickness (cm) | Density ($g.cm^{-3}$) |
|---|---|---|---|---|---|---|
| 0%LC-LLZO | 0.13 | 2 | 1.4148 | 0.2783 | 0.0465 | 3.8069 |
| 5D-LLZO | 0.29 | 2 | 1.3622 | 0.2746 | 0.0482 | 3.9091 |
| 1%LC-LLZO | 0.47 | 2 | 1.4024 | 0.3055 | 0.0504 | 3.9241 |
| 5%LC-LLZO | 0.48 | 2 | 1.4132 | 0.3027 | 0.0487 | 3.9626 |

* The Zr concentration was fixed to 2.

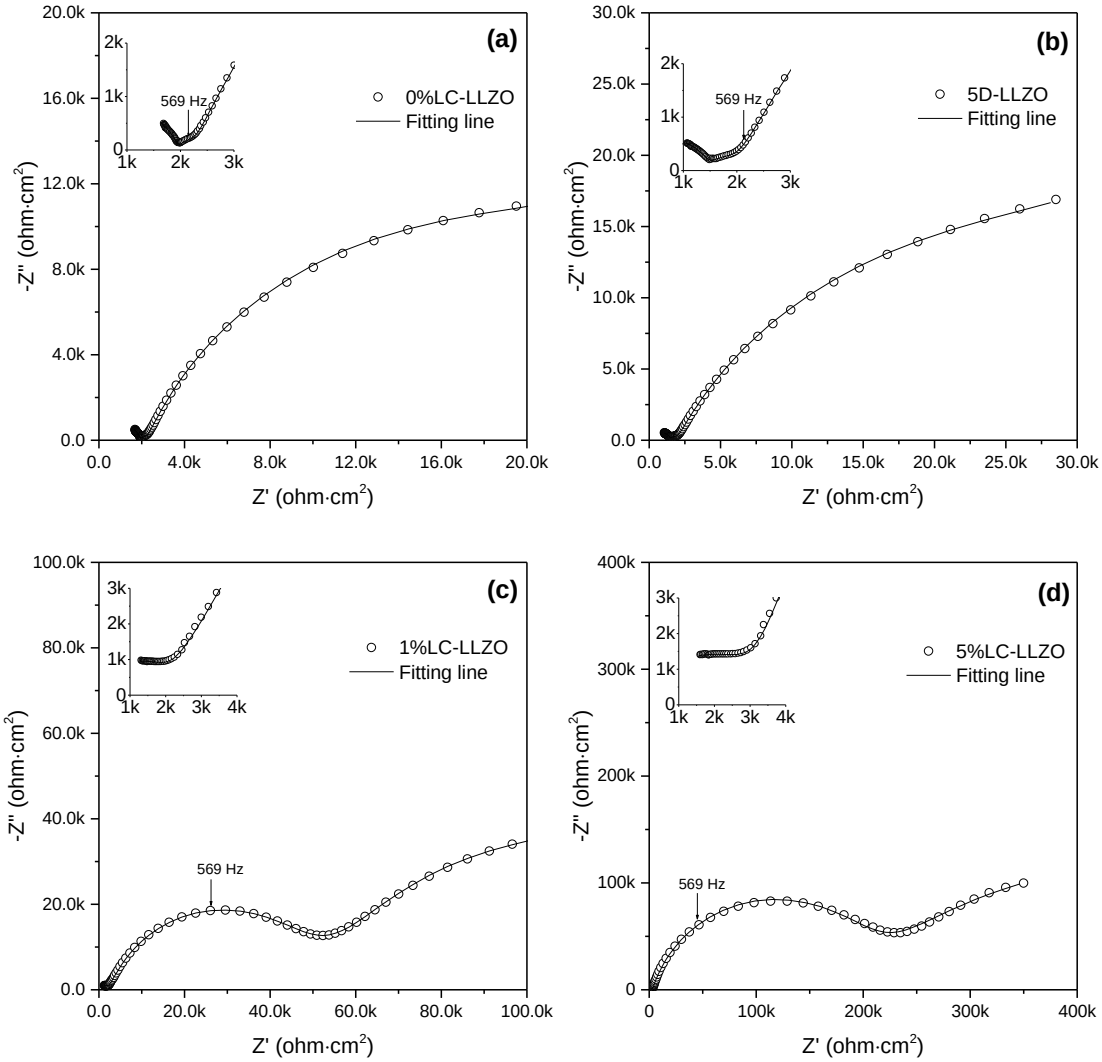


**Figure 4**. Impedance plots of $Li_7La_3Zr_2O_{12}$ obtained under different conditions. The solid line represents simulated data with an equivalent circuit consisting of $(R_gQ_g)(R_{gb}Q_{gb})(R_{el}Q_{el})Q$ (where R represents resistance, Q is the constant phase element, the subscripts g, gb and el refer to the grain, grain boundary, and electrode, respectively).

The elemental concentration in the pellets was also detected by ICP and the results are listed in Table 1. Apparently, the Al content in 0%LC-LLZO, 5D-LLZO, 1%LC-LLZO and 5%LC-LLZO are increased in the pellets, further confirming the formation of Al-containing compounds. Besides, we

calculated the density of the obtained pellets based on the measured dimensions and mass, as shown in Table 1. All the samples with $Li_2CO_3$ in advance (5D-LLZO, 1% LC-LLZO, 5%LC-LLZO) exhibit slightly higher density compared with the pristine sample, indicating that the formed Li-Al-O may fill into the grain boundary, resulting in much compact contact of the particles.

The grain and grain boundary resistance of the $Li_7La_3Zr_2O_{12}$ pellets were determined by AC-impedance and shown in Figure 4. A partial semicircle appeared in the high-frequency range, a complete semicircle in the middle-frequency and another semicircle appeared in the low-frequency range were observed in Nyquist plots for all the samples. The first semicircle at high frequency range can be attributed to the grain resistance ($R_g$), while the complete semicircle at middle frequency range ascribes to the resistance from grain boundary ($R_{gb}$). Electronic conductivities of each pellets were calculated based on equation 4.

$$\sigma = d/RA \qquad (4)$$

Where *d*, A are the thickness and area of the pellets, respectively, and R is the fitted resistance from the impedance plots. The calculated data are listed in Table 2, while some preliminary results can be obtained from the conductivity results of the pellets. Compared with the pristine 0%LC-LLZO, the 5D-LLZO sample exhibit the highest grain conductivity, indicating that minute Al-doping can improve the conductivity of the bulk particle, however, with more Al dopant embedded into the bulk particle, the grain conductivity decreased. The electronic conductivities of the grain boundary decrease regularly as more Al-containing impurities detected, indicating the negative effects of these impurities. Anyway, when it comes to the total electron conductivity of the pellets, it can be seen the 5D-LLZO exhibit the highest value, indicating proper Al element is helpful in the performance improvement.

**Table 2.** Impedance data of the $Li_7La_3Zr_2O_{12}$ pellets

| Sample ID | $\sigma_{grain}$ (S cm$^{-1}$) | $\sigma_{grain\ boundary}$ (S cm$^{-1}$) | $\sigma_{total}$ (S cm$^{-1}$) |
|---|---|---|---|
| 0%LC-LLZO | $2.38\times10^{-5}$ | $1.71\times10^{-4}$ | $2.09\times10^{-5}$ |
| 5D-LLZO | $3.27\times10^{-5}$ | $1.02\times10^{-4}$ | $2.48\times10^{-5}$ |
| 1%LC-LLZO | $3.18\times10^{-5}$ | $1.16\times10^{-6}$ | $1.12\times10^{-6}$ |
| 5%LC-LLZO | $1.75\times10^{-5}$ | $1.75\times10^{-7}$ | $1.73\times10^{-7}$ |

## 4. DISCUSSION

It is reported in previous papers that the Li-Al-O eutectic liquid have great effects on the sintering process of final LLZO, resulting in increased pellet density [26-28], which is also verified in this research. The formed Li-Al-O eutectic liquid formed at the grain boundaries in the pellet sintering process due to the lower energy sites at the grain boundary for solute atoms than in the bulk. Besides, the formation of amorphous Li-Al-O phase in the grain boundary can also facilitate the sintering of LLZO, thus blocking the Li loss at high temperature [29-30].

The extra $Li_2CO_3$ leads to the formation of $LiAlO_2$ impurity, results in denser ceramics, but more $Li_2CO_3$ also induce phase transformation from cubic phase to tetragonal one. The cubic phase of LLZO is usually stabilized by strict Li vacancy [31], since extra Al element is helpful in creating Li vacancy,

more Li vacancy from excess Al element will lead to instability of the cubic phase. Results from our research suggests that even excess $Li_2CO_3$ is usually added to offset the Li loss during the pellet sintering process, however, the excess amount should be regulated strictly to balance the pellet density as well as the cubic phase stabilization.

## 5. CONCLUSION

In this paper, we made some investigations on the $Li_2CO_3$ additives on the performance of LLZO solid electrolyte. Results indicate that extra $Li_2CO_3$ will increase the formation of Al-contained impurities, which gathered at the grain boundaries in the sintered electrolyte. The formed Al-contained impurities have great effects on the morphology as well as the electronic conductivities of the pellets due to the phase transformation from cubic to tetrahedron, which should be paid more attention in the electrolyte preparation process. The Al contamination from crucible arise from extra $Li_2CO_3$ will occur under a lower concentration of $Li_2CO_3$ (exposing the powder in air for 5 days), thus resulting in poor reproducibility and controllability in LLZO from solid-state synthesis.

ACKNOWLEDGEMENT
This work was financially supported by Key Platform and Major Scientific Research Project from Education Department of Guangdong Province (2017GkQNCX044).

## References

1. V. Thangadurai, S. Narayanan, D. Pinzaru, *Chem. Soc. Rev.*, 43 (2014) 4714-4727.
2. S. Stramare, V. Thangadurai, W. Weppner, *Chem. Mater.*, 15 (2003) 3974-3990.
3. Q. Liu, Z. Geng, C.P. Han, Y.Z. Fu, S. Li, Y.B. He, F.Y. Kang, B.H. Li, *J. Power Sources*, 389 (2018) 120-134.
4. C. L. Tsai, V. Roddatis, C. V. Chandran, Q. L. Ma, S. Uhlenbruck, M. Bram, P. Heitjans, O. Guillon, *ACS Appl. Mater. Interfaces*, 8 (2016) 10617-10626.
5. N. Kamaya, K. Homma, Y. Yamakawa, M. Hirayama, R. Kanno, M. Yonemura, T. Kamiyama, Y. Kato, S. Hama, K. Kawamoto, A. Mitsui, *Nat. Mater.*, 10 (2011) 682-686.
6. R. Muragan, V. Thangadurai, W. Wappner, *Chem. Int. Ed.*, 46 (2007) 7778-7781.
7. W.H. Xia, B.Y. Xu, H.N. Duan, Y.P. Guo, H.M. Kang, H. Li, H.Z. Liu, *ACS Appl. Mater. Interfaces*, 8 (2016) 5335-5342.
8. X. Huang, Y. Lu, H. Guo, Z. Song, T. Xiu, M.E. Badding, Z. Wen, *ACS Applied Energy Materials*, 1 (2018) 5355-5365.
9. Y. T. Li, X. Chen, A. Dolocan, Z. M. Cui, S. Xin, L. G. Xue, H. H. Xu, K. Park, J. B. Goodenough, *J. Am. Chem.*, Soc. 140 (2018) 6448-6455.
10. P.C. Zhao, Y. Xiang, Y. Xu, Y.H. Wen, W.F. Zhang, X.Y. Zhu, M. Li, S.T. Zhang, H. Ming, Z.Q. Jin, G.P. Cao, *J. Power Sources*, 388 (2018) 25-31.
11. Y. Jin, P. McGinn, *J. Power Sources*, 196 (2011) 8683-8687.
12. K. K. Fu, Y. Gong, B. Liu, Y. Zhu, S. Xu, Y. Yao, W. Luo, C. Wang, S. D. Lacey, J. Dai, Y. Chen, Y. Mo, E. Wachsman, L. Hu, *Sci. Adv.*, 3 (2017) e1601659.
13. L. Buannic, B. Orayech, J. M. L. Del Amo, J. Carrasco, N. A. Katcho, F. Aguesse, W. Manalastas, W. Zhang, J. Kilner, A. Llordes, *Chem. Mater.*, 29 (2017) 1769-1778.
14. Y. Q. Li, Z. Wang, C. L. Li, Y. Cao, X. X. Guo, *J. Power Sources*, 248 (2014) 642-646.

15. T. T. Yang, Y. Li, W. W. Wu, Z. Z. Cao, W. Y. He, Y. F. Gao, J. R. Liu, G. R. Li, *Ceram. Int.*, 44 (2018) 1538-1544.
16. X. Huang, Y. Lu, Z. Song, K. Rui, Q. S. Wang, T. P. Xiu, M. E. Badding, Z. Y. Wen, *Energy Storage Mater.*, (2019).
17. H. Xie, J. A. Alonso, Y. Li, M. T. Fernández-Díaz, J. B. Goodenough, *Chem. Mater.*, 23 (2011) 3587-3589.
18. Y. X. Wang, W. Lai, *J. Power Sources*, 275 (2015) 612-620.
19. K. Liu, J. T. Ma, C. A. Wang, *J. Power Sources*, 260 (2014) 109-114.
20. G. Larraz, A. Orera, M. L. Sanjuan, *J. Mater. Chem. A*, 1 (2013) 11419-11428.
21. L. Cheng, C. H. Wu, A. Jarry, W. Chen, Y. F. Ye, J. F. Zhu, R. Kostecki, K. Persson, J. H. Guo, M. Salmeron, G. Y. Chen, M. Doeff, *ACS Appl. Mater. Interfaces*, 7 (2015) 17649-17655.
22. L. Cheng, M. Liu, A. Mehta, H. L. Xin, F. Lin, K. Persson, G. Y. Chen, J. C. Ethan, M. Doeff, *ACS Applied Energy Materials*, 1 (2018) 7244-7252.
23. R. H. Brugge, A. K. O. Hekselman, A. Cavallaro, F. M. Pesci, R. J. Chater, J. A. Kilner, A. Aguadero, *Chem. Mater.*, 30 (2018) 3704-3713.
24. N. S. Kulkarni, T. M. Besmann, K. E. Spear, *J. Am. Ceram. Soc.*, 91 (2008) 4074-4083.
25. S. Smetaczek, A. W. Wachter, R. Wagner, D. Rettenwander, G. Amthauer, L. Andrejs, S. Taibl, A. Limbeck, J. Fleig, *J. Mater. Chem. A*, 7 (2019) 6818-6831.
26. Y. Matsuda, A. Sakaida, K. Sugimoto, D. Mori, Y. Takeda, O. Yamamoto, N. Imanishi, *Solid State Ionics*, 311 (2017) 69-74.
27. P. C. Zhao, Y. Xiang, Y. Xu, Y. H. Wen, W. F. Zhang, X. Y. Zhu, M. Li, Z. Q. Jin, H. Ming, G. P. Cao, *Ceram. Int.*, 44 (2018) 9105-9111.
28. Y. T. Li, X. Chen, A. Dolocan, Z. M. Cui, S. Xin, L. G. Xue, H. H. Xu, K. Park, J. B. Goodenough, *J. Am. Chem. Soc.*, 140 (2018) 6448-6455.
29. M. Kotobuki, K. Kanamura, Y. Sato, T. Yoshida, *J. Power Sources*, 196 (2011) 7750-7754.
30. C. L. Tsai, Q. Ma, C.Dellen, S. Lobe, F. Vondahlen, A. Windmüller, D. Grüner, H. Zheng, S. Uhlenbruck, M. Finsterbusch, F. Tietz, R. D. Fattakhova, H. P. Bruchkremer, O. Guillon, *Sustainable Energy & Fuels*, 3 (2019). 280-291.
31. T. Thompson, J. Wolfenstine, J. L. Allen, M. Johannes, A. Huq, I. N. David, J. Sakamoto, *J. Mater. Chem. A*, 33 (2014) 13431-13436.